Raman Measurements of Thermal Transport in Suspended Monolayer Graphene of Variable Sizes in Vacuum and Gaseous Environments

Shanshan Chen,[†,‡] Arden L. Moore,[†] Weiwei Cai,[†,‡] Ji Won Suk,[†] Jinho An,[†] Columbia Mishra,[†] Charles Amos,[†] Carl W. Magnuson,[†] Junyong Kang,[‡] Li Shi,[†,*] and Rodney S. Ruoff[†,*]

[†]Department of Mechanical Engineering and the Texas Materials Institute, The University of Texas at Austin, Austin, Texas 78712, United States, and [‡]Department of Physics, Fujian Key Laboratory of Semiconductor Materials and Applications, Xiamen University, Xiamen 361005, China

ABSTRACT Using micro-Raman spectroscopy, the thermal conductivity of a graphene monolayer grown by chemical vapor deposition and suspended over holes with different diameters ranging from 2.9 to 9.7 μm was measured in vacuum, thereby eliminating errors caused by heat loss to the surrounding gas. The obtained thermal conductivity values of the suspended graphene range from (2.6 ± 0.9) to (3.1 ± 1.0) × 10^3 $Wm^{-1}K^{-1}$ near 350 K without showing the sample size dependence predicted for suspended, clean, and flat graphene crystal. The lack of sample size dependence is attributed to the relatively large measurement uncertainty as well as grain boundaries, wrinkles, defects, or polymeric residue that are possibly present in the measured samples. Moreover, from Raman measurements performed in air and CO_2 gas environments near atmospheric pressure, the heat transfer coefficient for air and CO_2 was determined and found to be (2.9 +5.1/−2.9) and (1.5 +4.2/−1.5) × 10^4 $Wm^{-2}K^{-1}$, respectively, when the graphene temperature was heated by the Raman laser to about 510 K.

KEYWORDS: graphene · thermal conductivity · thermal boundary conductance · Raman spectroscopy · measurements

Thermal transport in graphene has received increasing attention in recent years because of its potential for thermal management applications. By using a noncontact optical technique where the temperature of the optically heated graphene was determined from the Raman G peak shift, the near-room temperature thermal conductivity of suspended graphene was recently measured to be between (4.84 ± 0.44) to (5.30 ± 0.48) × 10^3 $Wm^{-1}K^{-1}$.[1,3] These values, obtained on a suspended monolayer graphene flake produced by using mechanical exfoliation, are in excess of the thermal conductivity of carbon nanotubes[4−8] and diamond.[9] However, it was suggested in a recent work that the ultrahigh thermal conductivity values reported earlier were caused by an overestimated optical absorption and that the thermal conductivity of a ~44 μm diameter suspended graphene monolayer is about 600 $Wm^{-1}K^{-1}$ when the optical absorption of the Raman laser beam raises the center of the monolayer to a temperature of about 660 K, which was measured from the anti-Stokes to Stokes ratio of the Raman scattering signals.[10] At the same time, the thermal conductivity of a graphene monolayer grown by chemical vapor deposition (CVD) and suspended over a 3.8 μm diameter hole was measured to decrease from (2.5 ± 1.1) to (1.4 ± 0.5) × 10^3 $Wm^{-1}K^{-1}$ when the graphene temperature measured based on the Raman G peak shift of the optically heated graphene increased from about 350 to about 500 K.[11] This work suggested the importance of determining the temperature dependence of the graphene thermal conductivity as well as the need to measure the laser beam size for accurate Raman measurement of the graphene thermal conductivity in the Corbino membrane geometry.

While an electrical resistance thermometer-based method has recently been employed to measure thermal transport in supported graphene,[12] similar methods have not been reported for suspended graphene because of the difficulty in sample preparation compared to Raman measurements. On the other hand, the accuracy of the Raman-based measurements is limited by the uncertainty of the measured optical absorption as well as the temperature sensitivity of the optical technique. While progress has been made to address these issues in Raman measurements of thermal transport in suspended graphene,[2,10,11] all these measurements have been conducted in air. A recent Raman measurement of thermal transport in

*Address correspondence to r.ruoff@mail.utexas.edu, lishi@mail.utexas.edu.

Received for review October 27, 2010 and accepted December 06, 2010.

Published online December 16, 2010. 10.1021/nn102915x

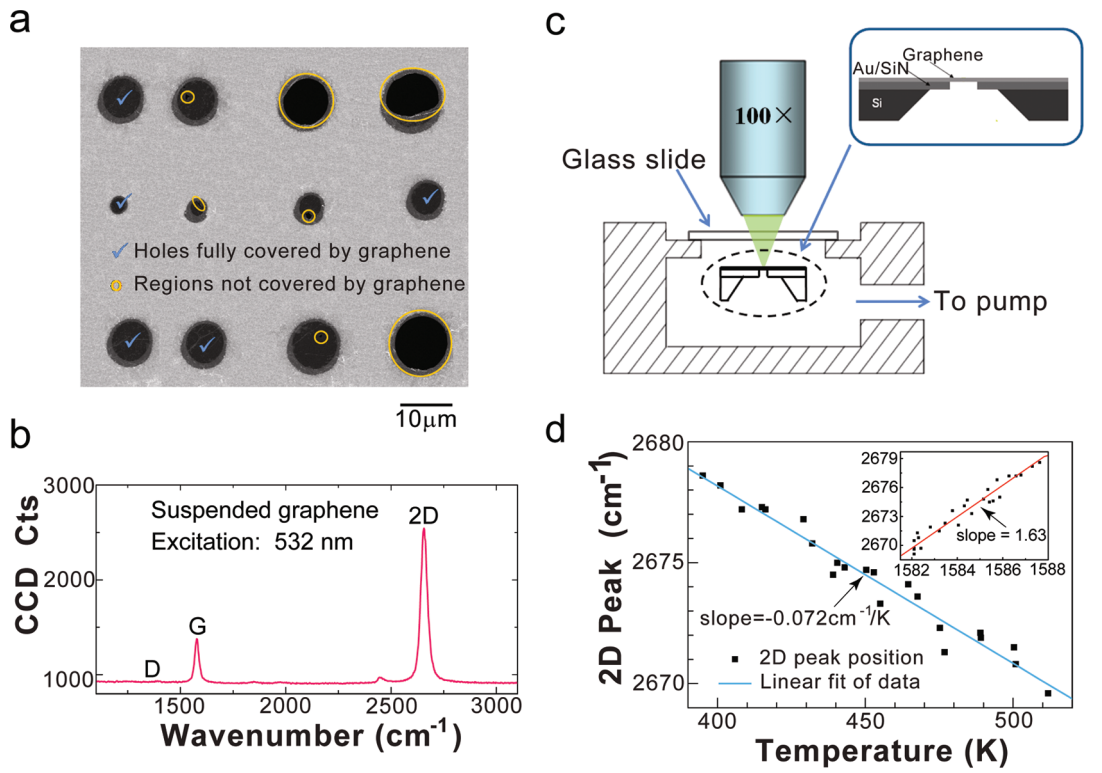

Figure 1. (a) SEM image of suspended graphene on a Au-coated SiN_x porous membrane. (b) Raman spectra of the suspended graphene showing the G and 2D peaks features characteristic of single-layer graphene. (c) Schematic of the experimental setup for thermal transport measurement of suspended graphene. (d) Temperature dependence of the 2D peak frequency for monolayer graphene. The inset shows the relationship between the G and 2D peak shifts.

likely defective carbon nanotubes has revealed that an appreciable fraction of optical heating was dissipated to the surrounding gases when the measurement was conducted with the nanotube in a gas environment.[13] Hence, this finding raises a critical question regarding whether the reported high thermal conductivity of suspended graphene could have consisted of large errors caused by heat dissipation to the surrounding air. Besides this critical question regarding the validity of the reported values, there exists an intriguing fundamental question regarding whether the lattice thermal conductivity of 2D suspended graphene would increase with lateral size because of an increasing contribution from the long-wavelength phonons that are cut off in finite-size graphene, as suggested by theoretical calculations.[2,14−16]

To address these two critical questions, here we report Raman measurements of graphene grown by CVD and subsequently suspended over holes with diameters ranging from 2.9 to 9.7 μm in vacuum, air, and CO_2 environments. From the measurements in vacuum, we obtain thermal conductivity values of (2.6 ± 0.9) to (3.1 ± 1.0) × 10^3 Wm^{-1} K^{-1} in different samples near 350 K, which are still higher than the reported experimental basal plane values for graphite. The obtained thermal conductivity values do not show clear size dependence in these CVD graphene samples. Moreover, the additional measurements in gases allow us to determine the gas heat transfer coefficient and compare the results to those calculated from kinetic and diffusion theories.

The sample used in the thermal measurement was large-area monolayer graphene grown on 25 μm thick Cu foil using a CVD method.[17−19] Graphene was later transferred to a low-stress silicon nitride (SiN_x) membrane substrate with a series of holes of diameters ranging from 2 to 10 μm. Figure 1a shows the scanning electron microscopy (SEM) image of suspended graphene on the substrate after transfer. Many of the holes were not covered by graphene, whereas a few holes were fully covered by graphene. A Raman spectrum typical of those obtained from the graphene monolayer fully suspended over one of the chosen holes is shown in Figure 1b, and it does not contain a D peak. The measured optical power transmitted through the uncovered holes and the holes fully covered by graphene, *i.e.*, P_{empty} and $P_{graphene}$, was used to determine the optical absorption by the graphene as $Q = P_{empty} - P_{graphene}$. The obtained optical absorption is 3.4 ± 0.7% at 532 nm wavelength for nine measurements of five samples.

To eliminate heat loss to surrounding gases during the thermal conductivity measurement as well as to allow for measurement in various gas environments, the prepared sample was placed into a small stainless steel vacuum chamber (Figure 1c) that was attached to a mechanical pump and a pressure gauge. Because both sides of the graphene sample are connected *via* open space in the chamber as well as holes in the SiN_x mem-

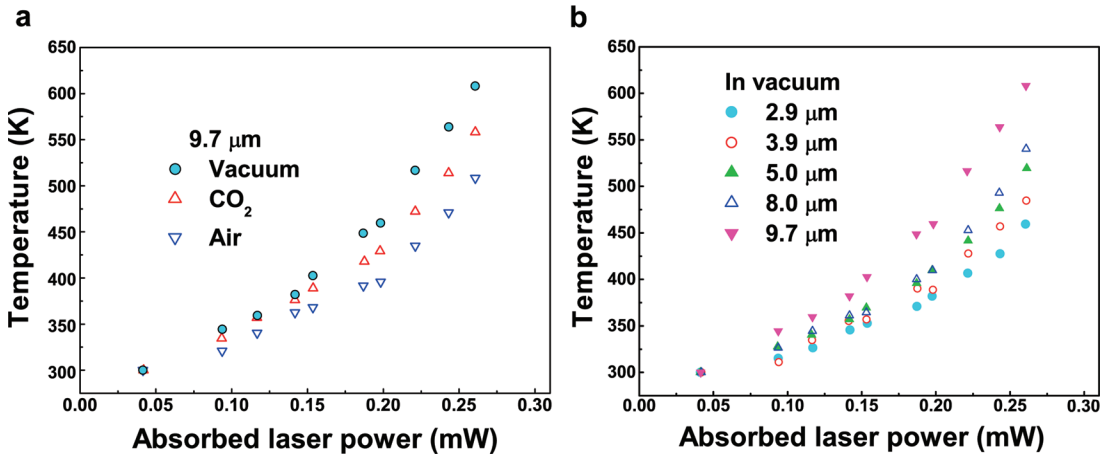

Figure 2. The 2D peak shift measured at the center of the suspended graphene as a function of the absorbed laser power for (a) 9.7 μm diameter suspended graphene sample in vacuum, CO_2, and air; and (b) 2.9, 3.9, 5.0, 8.0, and 9.7 μm diameter suspended graphene samples in vacuum.

brane that were not covered by graphene, no pressure difference was present to deflect the suspended graphene membrane during the measurement at different pressures. Additional details of the measurement can be found in the Methods Section.

RESULTS AND DISCUSSION

During the thermal measurement, a 532 nm laser beam was focused using the 100× objective lens on the center of the suspended graphene. The temperature rise in the heated graphene causes a red-shift of the Raman peak because of increased anharmonic scattering of those optical phonons that are active in the Raman scattering processes.[20,21] It has been shown that the red-shift of the Raman G peak of graphene linearly depends on the sample temperature.[11,22] For the case of optical heating, the temperature determined from the Raman G peak shift was found to be comparable to the temperature of zone-center optical phonons determined from the anti-Stokes and Stokes ratio.[10] In our work, the relationship between the Raman G and 2D peak shifts and the graphene temperature rise was calibrated by performing a Raman measurement of the graphene sample placed on a heating stage with its temperature determined with a thermocouple.[4] On the basis of 22 measurements on suspended graphene areas, the Raman 2D peak down shifts with increasing stage temperature at a rate of $(7.2 \pm 0.2) \times 10^{-2}$ cm^{-1}/K (Figure 1d), which is larger than the corresponding $(4.4 \pm 0.3) \times 10^{-2}$ cm^{-1}/K value for the G peak (inset of Figure 1d). Because of the higher temperature sensitivity, the 2D peak shift is used to determine the graphene temperature when the graphene is heated by the Raman laser at different power and the stage is kept at ambient temperature, although G peak shifts have been used in other prior thermal measurements of graphene.[1−3,11]

Before thermal measurement, the vacuum chamber was pumped to 1.0×10^{-1} Torr. For measurements in gaseous environments, the chamber was filled with air or CO_2 to 760 and 700 Torr, respectively. Figure 2a shows the relationship between the measured graphene temperature rise and the absorbed laser power in vacuum, air, and CO_2 when the laser was focused with a 100× objective on the center of the sample suspended over a 9.7 μm diameter hole. The temperature rise at the center of the suspended graphene is clearly smaller in gases than that measured in vacuum, indicating measurable heat loss to the surrounding gas. In addition, the temperature rise was larger at the same absorbed laser power for graphene on holes with larger diameter, as shown in Figure 2b.

Here, we define $R_m \equiv (T_m - T_0)/Q$ as the measured thermal resistance of the graphene sample, where T_m is the graphene temperature measured by the Raman laser beam and T_0 is the substrate temperature of 300 K. Moreover, R_m contains a thermal resistance contribution from the graphene region in contact with the Au/SiN_x support, $R_c \equiv (T_1 - T_0)/Q$, and a contribution from the suspended graphene, $R_g \equiv (T_m - T_1)/Q$, where T_1 is the temperature at the edge of the suspended graphene. The thermal contact resistance was calculated using the sample geometries in this work and the values of Au−graphene thermal conductivity and the Au−graphene interface thermal conductance determined in a previous work for the supported graphene region.[11] From these values, the R_c contribution was found to be about 10% of R_m near 350 K for the 2.9 μm sample and decreases with increasing sample size to about 3% of R_m near 350 K for the 9.7 μm sample.

In flat, clean, and suspended 2D graphene single crystals, the mean free path of low-frequency acoustic phonons near the center of the Brillouin zone is only limited by the crystal size. For the Raman measurement of the finite-size suspended graphene monolayer, ballistic phonons with mean free paths comparable to the radius of the suspended graphene are not in local ther-

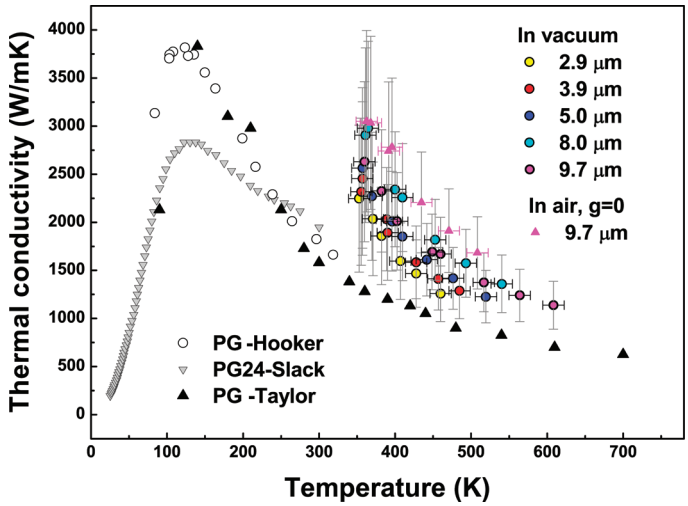

Figure 3. Thermal conductivity of the suspended CVD graphene as a function of the measured temperature of the graphene monolayer suspended in vacuum over holes of various diameters. Shown in comparison is the value obtained by neglecting heat loss to air or assuming $g = 0$ from a Raman measurement in air of a sample over a 9.7 μm hole and the literature thermal conductivity data of pyrolytic graphite samples as a function of temperature.[27−29]

mal equilibrium with diffusive phonons of higher frequencies and mean free paths shorter than the size of the suspended graphene. Moreover, the optical heating is coupled more strongly to diffusive phonons of higher frequencies than the ballistic phonons.[23] Consequently, the ballistic phonons are at a temperature lower than that of diffusive phonons and make little contribution to heat spreading. In addition, the temperature determined from the Raman G peak or 2D peak position is the anharmonic scattering temperature between the zone center or the zone-boundary optical phonons and diffusive acoustic phonons.[20,21] Hence, the Raman measurement mainly probes the temperature profile and the thermal transport of the diffusive phonons. As the radius of the suspended graphene monolayer increases to be larger than the mean free path of some long-wavelength phonons, these phonons become thermalized with diffusive phonons and begin contributing to heat spreading, resulting in a predicted increase in the thermal conductivity contribution from the diffusive phonons measured by the Raman technique.

For the case that the diffusive phonons probed by the Raman laser are thermalized locally within a scale comparable to the laser beam spot size, the as-defined R_g equals the diffusive thermal resistance ($R_{d,g}$) that is related to the thermal conductivity contribution (κ) from the diffusive phonons according to[11]

$$\kappa = \frac{\ln\left(\frac{R}{r_0}\right)}{2\pi t R_{d,g}}\alpha \qquad (1)$$

where R is the radius of the hole, $t = 0.335$ nm is the graphene monolayer thickness, and r_0 is the radius of the Gaussian laser beam. Without the factor α, eq 1 can be obtained from the diffusive thermal resistance expression of a cylindrical wall.[24] Based on the model discussed in detail in a recent work,[11] the α factor in eq 1 accounts for the Gaussian beam profile and ranges from 0.97 to 0.98 based on the suspended graphene radii R and the r_0 value of 0.27 ± 0.02 μm measured for the 100× objective lens, as discussed in the Methods Section. If the mean free paths of diffusive phonons are much larger than the laser beam size so that the diffusive phonons are not thermalized locally within the laser spot, R_g would consist of an additional ballistic resistance component ($R_{b,g}$), *i.e.*, $R_g \approx R_{d,g} + R_{b,g}$.[11,25]

With the calculated R_c subtracted from the R_m values measured in both vacuum and air to obtain R_g and with $R_{b,g}$ assumed to be negligible compared to $R_{d,g}$, we use eq 1 to calculate κ *versus* temperature T_m measured at the beam spot. The neglect of the ballistic resistance component $R_{b,g}$ could underestimate κ if the diffusive phonons are not thermalized locally within the laser spot. The as-calculated κ are shown in Figure 3, where the error in κ was calculated through the root-sum-square error propagation approach.[26] The error sources considered are the Raman peak position temperature calibration, temperature resolution of the Raman measurement method, and the uncertainty of the measured laser absorption. Of these error sources, the relative error in the laser absorption was by far the dominant contributor. The literature thermal conductivity data of pyrolytic graphite samples are also shown in Figure 3 for comparison.[27−29]

In Figure 3, the trend of decreasing κ with increasing T_m for the graphene samples is attributed to increased phonon−phonon scattering that becomes dominant over other scattering mechanisms with increased temperature.[23,30] Under a gray medium assumption where the phonon scattering mean free path is taken to be independent of phonon frequency, the phonon scattering mean free path at temperature 400 K is calculated from the thermal conductivity measured in vacuum to be in the range between 330 and 400 nm, which is comparable to the laser beam diameter. Hence, the diffusive phonons are mostly thermalized within the laser beam spot so that the effect of the ballistic resistance is not expected to be large, especially at higher temperatures with shorter phonon mean free paths.

The measured κ in vacuum does not show a clear sample size dependence compared to the measurement uncertainty. As discussed above, the predicted size-dependent κ in ideal 2D graphene is caused by the suppression of the contribution from the long-wavelength, long mean free path phonons in finite-size graphene monolayer.[14,15] In a previous work we reported that Cu-supported CVD graphene has a relatively high density of wrinkles and grain boundaries[19] that were identified by ^{13}C labeling and Raman mapping, from which graphene grain sizes ranging from 5

to 20 μm were observed. While isotope impurities and point defects are not effective in scattering long-wavelength phonons,[30] these long-wavelength phonons can be scattered effectively by the grain boundaries or wrinkles as well as polymer residue on the graphene. These scattering mechanisms as well as the relatively large uncertainty of the measured κ have obscured the predicted size-dependent κ in clean, flat, 2D graphene single crystal, where the mean free path of long-wavelength phonons is only limited by the crystal size.[2,14,15] Although these nonideal scattering processes limit the mean free path of long-wavelength phonons, the aforementioned 330−400 nm value for the phonon mean free path is still rather long, giving rise to the higher κ in the CVD graphene than the highest value reported for graphite.

For Raman measurement in a gas environment, the temperature (T) distribution of the diffusive phonons in graphene can be obtained from the following heat diffusion equation in the cylindrical coordinate

$$\frac{1}{r}\frac{d}{dr}\left(r\frac{dT}{dr}\right) - \frac{2g}{\kappa t}(T - T_a) + \frac{\dot{q}'''}{\kappa} = 0 \qquad (2)$$

where T_a is the ambient temperature, r is the radial position measured from the center of the laser beam, κ is the thermal conductivity of the suspended graphene, $\dot{q}'''$ is the localized heat generation from the laser beam, and g is the heat transfer coefficient per unit area between the graphene and the surrounding gas molecules. By solving eq 2 with appropriate boundary conditions, the temperature of the diffusive phonons measured by the Raman laser may be determined for given values of Q, κ, and g. This is similar to the analysis used in our previous work to analyze the thermal interface conductance between supported graphene and a Au film.[11] Here, with the absorbed laser power Q measured directly and κ determined from the Raman measurement in vacuum, g was adjusted such that the measured temperature in the model matched that of the experiment at each laser power. The as-obtained gas heat transfer coefficients in air and CO_2 are shown in Figure 4 with the uncertainty in κ propagated into the obtained values of g.

The thermal resistance of the surrounding gas R_{gas} has both a boundary resistance component R_b at the graphene−gas interface and a diffusive component R_d of the gas medium such that $R_{gas} = R_d + R_b$. The diffusive component can be estimated from the thermal resistance of an isothermal disk losing heat to a semi-infinite medium, specifically[31]

$$R_d = \frac{1}{4a\kappa_{gas}} \qquad (3)$$

where κ_{gas} is the thermal conductivity of the gas and a is the radius of the heated region of the graphene which would lie between r_0 and R. For this a range, the diffusive thermal resistances are estimated to be ~2×10^6 to 4×10^7 K W^{-1} for air and ~7×10^5 to 1×10^7 K W^{-1} for CO_2, respectively, at atmospheric pressure. At the lowest pressure of 1.0×10^{-1} Torr used in this work for the vacuum measurement, the intermolecule scattering mean free path of air molecules is estimated to be $l_m \sim 1$ mm, which is considerably smaller than the molecule boundary scattering mean free path l_b, which is close to the ~100 μm distance between the graphene sample and the glass cover slide of the vacuum chamber. For evaluating the magnitude of R_d under this rarefied gas condition, the kinetic theory and Matthiessen's rule[32] can be combined to yield

$$\kappa_{gas} \approx Cv(l_m^{-1} + l_b^{-1})^{-1}/3 \qquad (4)$$

where C is the specific heat of the gas in question, $v = (3k_BT_{gas}/m)^{1/2}$ is the root-mean-square velocity of gas molecules with a molecular weight of m and temperature T_{gas}, and k_B is the Boltzmann constant. Based on this approximation, κ_{gas} and R_d are expected to be reduced and increased, respectively, by about 1 order of magnitude at the vacuum level of 1.0×10^{-1} Torr compared to the corresponding values at atmospheric pressure.

The thermal boundary resistance is given by

$$R_b = \frac{1}{g_b A_{graphene}} \qquad (5)$$

where g_b is the gas−graphene thermal boundary conductance per unit area and $A_{graphene}$ is the area of the suspended graphene. The gas−graphene thermal boundary conductance g_b can be calculated from the kinetic theory by

$$g_b = \beta(v/4)C \qquad (6)$$

where β is the molecular accommodation coefficient and P_{gas} and T_{gas} are the pressure and temperature of the gas molecules, respectively. For diatomic molecules, such as O_2 or N_2 which dominate the composition of air, $C = 5nk_B/2$, where $n = P_{gas}/k_BT_{gas}$ is the number density of air molecules. For a triatomic molecule such as CO_2 at near-ambient conditions, $C = 7nk_B/2$. The maximum thermal boundary conductance for both cases occurs when $\beta = 1$. This upper limit at atmospheric pressure is plotted along with the experimentally derived values of g for air in Figure 4a and for CO_2 in Figure 4b. The thermal boundary resistance is inversely proportional to pressure. For the maximum boundary conductance calculated using $\beta = 1$ with eq 6, the minimum thermal boundary resistances are estimated to be 1×10^9 K W^{-1} for the vacuum measurement and 1×10^5 K W^{-1} for the air and CO_2 measurements. Thus, the thermal boundary resistance dominates the diffusive resistance for the vacuum measurement and is comparable to or slightly smaller than the diffusive resistance for the air and CO_2 measurements.

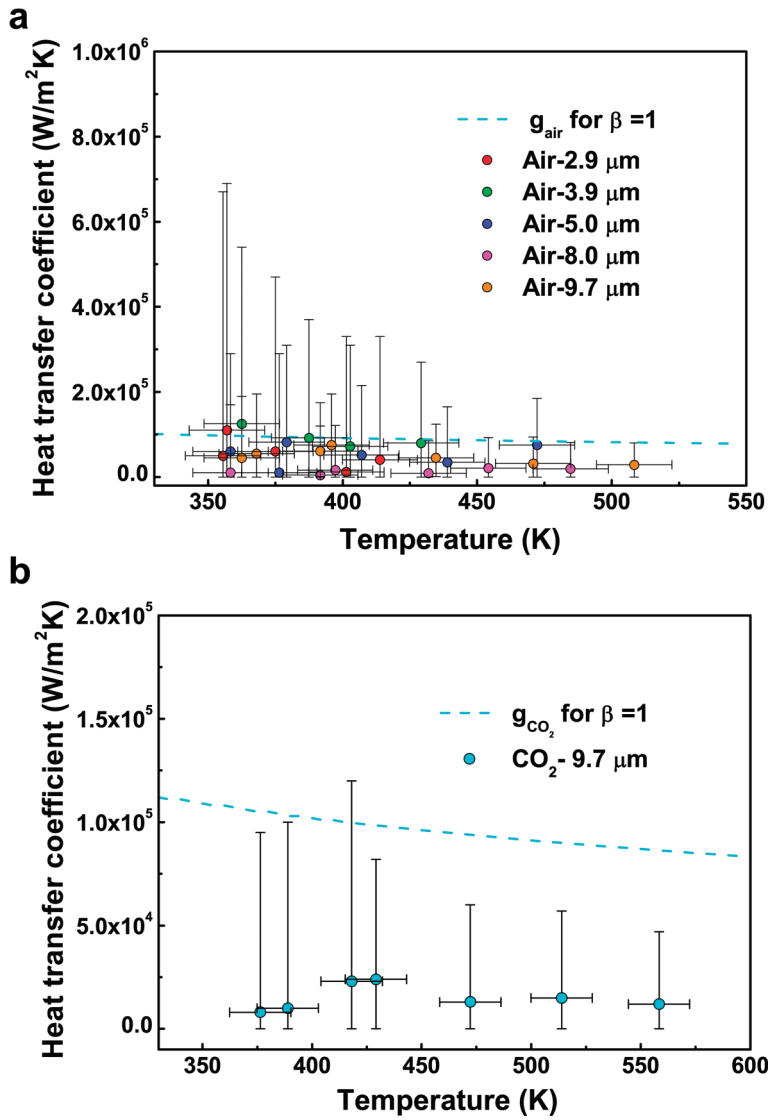

Figure 4. Gas heat transfer coefficient as a function of the measured temperature of graphene suspended over holes of various diameters in air (a) and in CO_2 for a 9.7 μm diameter sample (b). Shown in comparison are the maximum thermal boundary conductance values calculated from the kinetic theory.

For the air data near 350 K where the experimental uncertainty in κ is large, the associated uncertainty in g overlaps the upper limit of g_b set by $\beta = 1$. This is also seen at higher temperatures for the samples with diameters of 5 μm or smaller, where the area over which heat loss to gas occurs is rather small and thus gives rise to large uncertainty in the obtained g. However, for the two largest samples of 8.0 and 9.7 μm diameter, respectively, above about 425 K, the upper limit of the experimental uncertainty is comparable to or below the values set by kinetic theory for $\beta = 1$. This same result is shown even more clearly in Figure 4b for measurements performed in CO_2 gas. The finding of $g < g_b$ can be attributed to the presence of the non-negligible R_d in the atmospheric gas as well as a possible $\beta < 1$.

If heat loss to the gas is ignored (*i.e.*, $g = 0$ is assumed) for Raman measurement in air of the largest sample size of 9.7 μm diameter, eq 1 is the solution to eq 2 and would yield a κ value that is 14−40% higher than that obtained from measurements in vacuum. Therefore, the parasitic heat loss to surrounding gas can indeed cause measurable errors in the obtained κ, although the error is comparable to the measurement uncertainty propagated from those in the temperature and the optical heating measurements.

CONCLUSIONS

These Raman measurements performed in vacuum, air, and CO_2 gas environments show that parasitic heat loss to surrounding gas can cause measurable errors in the obtained thermal conductivity, although the error is comparable to those caused by uncertainties in the measured temperature and the optical absorption. Together with the appreciable measurement uncertainty of the Raman technique, scattering of long-wavelength phonons by grain boundaries, wrinkles, and possibly polymer residues on the suspended CVD graphene has obscured the predicted size-dependent thermal con-

ductivity for clean, suspended, and flat graphene crystals. Nevertheless, the measured thermal conductivity values of the suspended graphene in vacuum range from (2.6 ± 0.9) to (3.1 ± 1.0) × 10^3 Wm^{-1} K^{-1} near 350 K, which is still higher than the reported basal plane thermal conductivity of highly oriented pyrolytic graphite. In addition, Raman measurements performed in air and CO_2 gas environments allow us to determine the heat transfer coefficient for both gases to be (2.9 +5.1/−2.9) and (1.5 +4.2/−1.5) × 10^4 $Wm^{-2}K^{-1}$ for air and CO_2, respectively, at about 510 K and near the atmospheric pressure.

METHODS

Large-area high-quality monolayer graphene was grown on 25 μm thick Cu foil using a CVD method that we demonstrated recently.[17−19] The surface of the graphene-on-Cu was spin-coated with a thin layer of poly(methyl methacrylate) (PMMA) followed by curing. After the Cu substrate was dissolved in an $Fe(NO_3)_3$ solution (1M), the PMMA/graphene film was transferred to the Au-coated surface of a 300 nm thick, 0.5 × 0.5 mm^2, low-stress silicon nitride (SiN_x) membrane supported on a circular 3 × 3 mm^2 silicon frame.[11,33] A series of holes with diameters ranging from 2 to 10 μm were cut into the Au-coated SiN_x membrane by focused ion beam (FEI Strata DB235 SEM/FIB) prior to the graphene transfer. For graphene transfer, the graphene/PMMA film was lifted up from the copper-etching solution and moved onto a water surface for rinsing. SiN_x substrates were placed in a fixture within the water. The graphene/PMMA film was laid down on the SiN_x substrates. The whole sample was dried in vacuum, which gave a good contact between graphene and the substrate. Liquid PMMA in chlorobenzene was dropped on top of the substrate to dissolve some of the thin solid PMMA and relax the underlying graphene. Subsequently, the sample was dried in air. After the dried PMMA was removed using acetone, suspended graphene on the SiN_x substrate was obtained.

The prepared sample was loaded into a small stainless steel vacuum chamber that was attached to a mechanical pump and a pressure gauge (see Figure 1c). In order to match with the short working distance (~250 μm) of the 100× objective used in our micro-Raman apparatus, the top of the vacuum chamber was sealed with a 100 μm thick glass cover slide by vacuum grease. The vacuum chamber can be evacuated to a pressure of 1.0 × 10^{-1} Torr using the mechanical pump.

SEM images were taken with an FEI Quanta-600 FEG Environmental SEM using a voltage of 30 keV. Raman scattering experiments have been carried out at room temperature using the 532.0 nm line of the Ar-ion laser (~50 mW power) as the excitation source and a confocal micro-Raman setup (WITec Alpha-300) equipped with a 100× microscope objective. The Raman laser beam profile was measured by performing a Raman mapping across a smooth cleaved edge of a Si substrate placed in the same position as graphene in the vacuum chamber, as reported previously.[4] The measured beam intensity profile for the 100× objective can be fitted with a Gaussian function of $\exp(-r^2/r_0^2)$, where r is the distance measured from the center of the beam and r_0 was found from the fitting to be 0.27 ± 0.02 μm, with the uncertainty dominated by the pixel resolution of the obtained Raman map. This value is slightly larger than the value of 0.17 ± 0.02 μm found previously[11] without the presence of the thin glass slide between the objective lens and the sample.

Acknowledgment. This work was supported in part by The University of Texas at Austin, the Texas Nanotechnology Research Superiority Initiative (TNRSI)/SWAN, the Office of Naval Research awards N00014-10-1-0581, the Department of Energy Office of Science award DEFG02-07ER46377, and the National Science Foundation award CBET-0553649. S. Chen is supported by the China Scholarship Council Fellowship, the National Basic Research Program of China (2011CB925600) and the National Natural Science Foundation of China (60827004, 90921002, and 60776066).

REFERENCES AND NOTES

1. Balandin, A. A.; Ghosh, S.; Bao, W. Z.; Calizo, I.; Teweldebrhan, D.; Miao, F.; Lau, C. N. Superior Thermal Conductivity of Single-Layer Graphene. *Nano Lett.* **2008**, *8*, 902–907.
2. Ghosh, S.; Nika, D. L.; Pokatilov, E. P.; Balandin, A. A. Heat Conduction in Graphene: Experimental Study and Theoretical Interpretation. *New J. Phys.* **2009**, *11*, 095012.
3. Ghosh, S.; Calizo, I.; Teweldebrhan, D.; Pokatilov, E. P.; Nika, D. L.; Balandin, A. A.; Bao, W.; Miao, F.; Lau, C. N. Extremely High Thermal Conductivity of Graphene: Prospects for Thermal Management Applications in Nanoelectronic Circuits. *Appl. Phys. Lett.* **2008**, *92*, 151911.
4. Kim, P.; Shi, L.; Majumdar, A.; McEuen, P. L. Thermal Transport Measurements of Individual Multiwalled Nanotubes. *Phys. Rev. Lett.* **2001**, *87*, 215502.
5. Yu, C. H.; Shi, L.; Yao, Z.; Li, D. Y.; Majumdar, A. Thermal Conductance and Thermopower of an Individual Single-wall Carbon Nanotube. *Nano Lett.* **2005**, *5*, 1842–1846.
6. Fujii, M.; Zhang, X.; Xie, H.; Ago, H.; Takahashi, K.; Ikuta, T.; Abe, H.; Shimizu, T. Measuring the Thermal Conductivity of a Single Carbon Nanotube. *Phys. Rev. Lett.* **2005**, *95*, 065502.
7. Pettes, M. T.; Shi, L. Thermal and Structural Characterizations of Individual Single-, Double-, and Multi-Walled Carbon Nanotubes. *Adv. Funct. Mater.* **2009**, *19*, 3918–3925.
8. Pop, E.; Mann, D.; Wang, Q.; Goodson, K.; Dai, H. J. Thermal Conductance of an Individual Single-wall Carbon Nanotube above Room Temperature. *Nano Lett.* **2006**, *6*, 96–100.
9. Berman, R.; Foster, E. L.; Ziman, J. M. The Thermal Conductivity of Dielectric Crystals: The Effect of Isotopes. *Proc. R. Soc. London, Ser. A* **1956**, *237*, 344–354.
10. Faugeras, C.; Faugeras, B.; Orlita, M.; Potemski, M.; Nair, R. R.; Geim, A. K. Thermal Conductivity of Graphene in Corbino Membrane Geometry. *ACS Nano* **2010**, *4*, 1889–1892.
11. Cai, W. W.; Moore, A. L.; Zhu, Y. W.; Li, X. S.; Chen, S. S.; Shi, L.; Ruoff, R. S. Thermal Transport in Suspended and Supported Monolayer Graphene Grown by Chemical Vapor Deposition. *Nano Lett.* **2010**, *10*, 1645–1651.
12. Seol, J. H.; Jo, I.; Moore, A. L.; Lindsay, L.; Aitken, Z. H.; Pettes, M. T.; Li, X. S.; Yao, Z.; Huang, R.; Broido, D.; et al. Two-dimensional Phonon Transport in Supported Graphene. *Science* **2010**, *328*, 213–216.
13. Hsu, I. K.; Pettes, M. T.; Aykol, M.; Shi, L.; Cronin, S. B. The Effect of Gas Environment on Electrical Heating in Suspended Carbon Nanotubes. *J. Appl. Phys.* **2010**, *108*, 084307.
14. Klemens, P. G. Theory of Thermal Conduction in Thin Ceramic Films. *Int. J. Thermophys.* **2001**, *22*, 265–275.
15. Nika, D. L.; Ghosh, S.; Pokatilov, E. P.; Balandin, A. A. Lattice Thermal Conductivity of Graphene Flakes: Comparison with Bulk Graphite. *Appl. Phys. Lett.* **2009**, *94*, 203103.
16. Lindsay, L.; Broido, D. A.; Mingo, N. Flexural Phonons and Thermal Transport in Graphene. *Phys. Rev. B: Condens. Matter Mater. Phys.* **2010**, *82*, 115427.
17. Li, X. S.; Cai, W. W.; An, J. H.; Kim, S.; Nah, J.; Yang, D. X.; Piner, R.; Velamakanni, A.; Jung, I.; Tutuc, E.; et al. Large-Area Synthesis of High-Quality and Uniform Graphene Films on Copper Foils. *Science* **2009**, *324*, 1312–1314.
18. Li, X. S.; Cai, W. W.; Jung, I. H.; An, J. H.; Yang, D. X.; Velamakanni, A.; Piner, R.; Colombo, L.; Ruoff, R. S. Synthesis, Characterization, and Properties of Large-Area Graphene Films. *ECS Trans.* **2009**, *19*, 41–52.
19. Li, X. S.; Cai, W. W.; Colombo, L.; Ruoff, R. S. Evolution of Graphene Growth on Ni and Cu by Carbon Isotope Labeling. *Nano Lett.* **2009**, *9*, 4268–4272.

20. Basko, D. M.; Piscanec, S.; Ferrari, A. C. Electron-Electron Interactions and Doping Dependence of the Two-Phonon Raman Intensity in Graphene. *Phys. Rev. B: Condens. Matter Mater. Phys.* **2009**, *80*, 165413.
21. Bonini, N.; Lazzeri, M.; Marzari, N.; Maui, F. Phonon Anharmonicities in Graphite and Graphene. *Phys. Rev. Lett.* **2007**, *99*, 176802.
22. Calizo, I.; Balandin, A. A.; Bao, W.; Miao, F.; Lau, C. N. Temperature Dependence of the Raman Spectra of Graphene and Graphene Multilayers. *Nano Lett.* **2007**, *7*, 2645–2649.
23. Chen, G. *Nanoscale Energy Transport and Conversion*; Oxford University Press: New York, 2005.
24. Incropera, F. P.; Dewitt, D. P. *Fundamentals of Heat and Mass Transfer*, 5th ed.; J. Wiley & Sons: New York, 2002.
25. Chen, G. Nonlocal and nonequilibrium heat conduction in the vicinity of nanoparticles. *J. Heat Transfer* **1996**, *118*, 539–545.
26. Figliola, R. S.; Beasley, D. E. *Theory and Design for Mechanical Measurements;* John Wiley & Sons: New York, 2000.
27. Slack, G. A. Anisotropic Thermal Conductivity of Pyrolytic Graphite. *Phys. Rev.* **1962**, *127*, 694–701.
28. Taylor, R. The Thermal Conducivity of Pyrolytic Graphite. *Phil. Mag.* **1966**, *13*, 157–166.
29. Hooker, C. N.; Ubbelohd., Ar; Young, D. A. Anistropy of Thermal Conductance In Near-Ideal Graphene. *Proc. R. Soc. London, Ser. A* **1965**, *284*, 17.
30. Ziman, J. M. *Electrons and Phonons: The Theory of Transport Phenomena in Solids*; Clarendon Press: Oxford, 1960.
31. Incropera, F. P.; Dewitt, D. P. *Fundamental of Heat and Mass Transfer 6E*; John Wiley & Sons: New York, 2007.
32. Chen, G. *Nanoscale Energy Transport and Conversion*; Oxford University Press: New York, 2005; p 531.
33. Cai, W. W.; Zhu, Y. W.; Li, X. S.; Piner, R. D.; Ruoff, R. S. Large Area Few-Layer Graphene/Graphite Films as Transparent Thin Conducting Electrodes. *Appl. Phys. Lett.* **2009**, *95*, 123115.